Journal of Power Sources 255 (2014) 431–438

Contents lists available at ScienceDirect

Journal of Power Sources

journal homepage: www.elsevier.com/locate/jpowsour

Morphology studies on high-temperature polymer electrolyte membrane fuel cell electrodes

Florian Mack [a], Merle Klages [b], Joachim Scholta [b], Ludwig Jörissen [b], Tobias Morawietz [c], Renate Hiesgen [c], Dominik Kramer [a], Roswitha Zeis [a,*]

[a] Karlsruhe Institute of Technology, Helmholtz Institute Ulm, D-89081 Ulm, Germany
[b] Centre for Solar Energy and Hydrogen Research Baden-Wuerttemberg, Division 3, Electrochemical Energy Storage and Conversion, D-89081 Ulm, Germany
[c] University of Applied Sciences Esslingen, Department of Basic Science, D-73733 Esslingen, Germany

HIGHLIGHTS

- Steady-state cell performance is insensitive to electrode macrostructure variation.
- High surface wettability of the catalyst layer reduces the cell start-up time.
- Electrode microstructure has a major impact on the steady-state cell performance.
- Slow drying process of the catalyst slurry leads to a PTFE-rich electrode surface.

ARTICLE INFO

Article history:
Received 16 August 2013
Received in revised form
11 December 2013
Accepted 7 January 2014
Available online 15 January 2014

Keywords:
HT-PEM
PBI doped with phosphoric acid
X-ray microtomography
Atomic force microscopy (conductive mode)
Electrode morphology
Electrode preparation

ABSTRACT

The electrode morphology influences the properties and performance of polymer electrolyte membrane fuel cells (PEMFC). Here we report our studies of two different electrodes for high-temperature PEMFC prepared by spraying and coating and their impact on the fuel cell performance. Differences in 3D microstructure and adhesion between catalyst layer and gas diffusion layer (GDL) of the electrodes were studied with X-ray microtomography. Scanning electrode microscope investigations show hairline cracks between agglomerates on the surface of the sprayed electrode, whereas the coated electrode shows a network of shrinkage cracks in the catalyst layer. The distribution of the electrode binder polytetrafluoroethylene (PTFE) is related to the locally resolved conductivity, which was determined by scanning the electrode surfaces with a conductive atomic force microscopy (AFM) tip. The macrostructures of the sprayed and coated electrodes are different but contain similar pore structures. The coated electrode has a higher PTFE concentration on the top region, which tends to form a nonconductive and less wettable "skin" on the electrode surface and delays the start-up of the fuel cell. In contrast to low-temperature PEMFC, the electrode morphology has only a minor impact on the steady-state cell performance of high-temperature PEMFC.

1. Introduction

In recent years, the high-temperature polymer electrolyte membrane fuel cells (HT-PEMFC) have attracted increasing research interests. The benefits of operating the fuel cell at elevated temperatures (>120 °C) include improved catalyst activity, higher tolerance to impurities such as carbon monoxide in the hydrogen fuel, and much simplified thermal and water management of the system. Generally, the performance of HT-PEMFC is robust under a wide range of operating conditions. All these advantages make the HT-PEMFC ideally suited for applications such as stationary and auxiliary power units [1,2].

A conventional high-temperature membrane electrode assembly (HT-MEA) primarily consists of a polybenzimidazole (PBI) type membrane containing phosphoric acid and two gas diffusion electrodes (GDE), the anode and the cathode, attached to the two surfaces of the membrane. GDEs are usually prepared by spreading a suspension of carbon-supported platinum catalyst, solvent, and binder onto a gas diffusion layer (GDL), followed by drying. Because of the elevated operating temperature of HT-PEMs, polytetrafluoroethylene (PTFE) is often used as the binder material. The commonly used techniques to dispense the catalyst suspension include spraying [3] and coating [4].

* Corresponding author.
E-mail address: roswitha.zeis@kit.edu (R. Zeis).

0378-7753/$ – see front matter © 2014 Elsevier B.V. All rights reserved.
http://dx.doi.org/10.1016/j.jpowsour.2014.01.032

Although a great deal of effort has been devoted to cell performance optimization by altering individual components of the GDE [4–9], there are considerably fewer studies that investigate how these changes might affect the electrode morphology and subsequently impact the cell performance. There are some very limited studies to compare the influences of different catalyst layer deposition methods and electrode morphologies on the performance of GDEs for HT-PEMFC [10] and low-temperature PEMFC [11–15].

In the general field of PEMFCs, there exist a wide range of catalyst deposition methods [16], such as spraying [17], decal transfer [18], painting [10], screen printing [19], rolling [20], sputter deposition [21], coating [4] etc. For our study we selected the two most common methods for HT-PEMFCs, i.e., spraying and coating. With these two different techniques, significant differences in the electrode micro- and macrostructures are expected because the processes and the consistencies of the catalyst suspensions are distinctly different. Spraying is a layer-by-layer process using a relatively dilute catalyst suspension, while coating is a one-step process using a more concentrated and more viscous suspension.

To better understand how these different electrode morphologies affect the electrochemical properties of the GDEs, we conducted extensive studies employing a variety of advanced experimental techniques including X-ray microtomography, conductive atomic force microscopy, and scanning electron microscopy. To characterize the GDEs electrochemically, we fabricated MEAs using these electrodes and evaluated them in single cell tests.

X-ray microtomography is an emerging analytical technique, which is based on the same principle as the well-known X-ray computed tomography (CT) method for medical imaging. It measures variations in X-ray attenuation upon sample rotation to generate cross-sectional images of the samples at various depths into the material with high spatial resolution (0.7–26 μm/pixel) in a non-destructive fashion over large geometric volumes (on the order of 1 mm^3). Furthermore, variations in X-ray absorption also provide information on different phases/elements and their distribution within the sample. In fuel cell research, this technique has been used mainly for visualization of the morphology and water build-up in GDLs [17,22]. Complete MEAs were imaged by Pfrang et al. [23]. Very recently, Jhong et al. [11,12] employed X-ray microtomography to correlate the catalyst layer structures with the fuel cell performance. All these studies were performed for the low-temperature Nafion-based PEM fuel cells.

To investigate the PTFE distribution within the electrode, we performed measurements with atomic force microscopy (AFM). Besides morphology and topography, AFM is also capable of measuring the locally resolved conductivity of the sample. Thereby a Pt-coated AFM tip probes the current between the back and the top of the sample as its moves over its surface. The technique was used before to characterize low-temperature PEM fuel cell membranes and electrodes [24,25], and we find it is specially suited for HT-PEM electrodes due to the distinctive spherical shape of the nonconductive PTFE binder. Furthermore, we took scanning electron microscopy (SEM) images of the catalyst layers to complement our investigations. SEM is a valuable tool for visualization of the surface morphology and porosity of the electrodes.

2. Experimental

2.1. Preparation of GDEs via spraying and coating

Catalyst suspensions containing water (Millipore®), isopropanol, PTFE solution (60%, 3M), and 20% Pt/C (Heraeus) were used for the GDE preparation. The water content was adjusted to optimize the consistency of the suspension for different catalyst deposition processes, resulting in an “ink” for spraying and a “paste” for coating. The weight ratio of the suspension’s various compositions (water, isopropanol, PTFE solution, and carbon-supported catalyst) were (15:12:1:1) and (3:12:1:1) for the ink and paste, respectively. To produce a homogenous suspension, a magnetic stirrer was sufficient for mixing the ink, whereas an Ultra-Turrax® dispersing machine (IKA) was used for the paste.

In the next step, the paste was coated onto the microporous layer of a commercially available GDL (10BB, SGL Carbon) with an automated doctor blade technique. The drying process was at room temperature, first in a closed box for 24 h and then in open atmosphere until the weight was constant. The ink, on the other hand, was sprayed in multiple layers directly onto the microporous layer of the same GDL (also 10BB, SGL Carbon) at a substrate temperature of 80 °C. The distance between the spray head and the substrate was about 20 cm, the average drop size was below 0.5 mm, and each layer was dry after about 1 min. For this study, the catalyst loading was kept constant at around 1 mg cm^{-2}, which was calculated from the weight difference between the dried GDE and the GDL. All the GDEs had approximately the same PTFE content of circa 40% by weight.

2.2. Structural characterization of GDEs

2.2.1. Scanning electron microscopy (SEM)

The surface microstructures of the GDEs were studied using a scanning electron microscope (Merlin, Carl Zeiss). Depending on the magnification, the images were taken with an accelerating voltage between 8 and 15 kV. Because of their high intrinsic conductivity, the samples did not require additional conductive coating for SEM.

To image the cross-sections of the GDEs, a Nova Nanolab 200 (FEI) focused ion beam scanning electron microscopy (SEM/FIB) system was employed, which combines an ultra-high resolution field emission SEM with a focused ion beam (FIB) to etch the sample surface. In this microscope, an electron column placed above the sample stage enables imaging at high resolutions down to approximately 1 nm. The gallium-ion source for the FIB is mounted at an angle of 52° relative to the electron column. The SEM accelerating voltage was also between 8 and 15 kV. Due to the high cohesion between the particles and the material density, the sample pores were not filled before sputtering.

2.2.2. X-ray microtomography

Micro-CT 1172 (Skyscan) was used for visualization of the electrode internal structures with a resolution down to a few μm. The X-ray source had a variable accelerating voltage between 20 and 100 kV and a maximum power of 10 W. Lower-energy X-ray is suitable for light and porous materials such as carbon fibers of the GDL, whereas higher-energy is preferred for dense metal materials like platinum in the catalyst layer. The samples were circular specimens with a diameter of 4 mm. They were punched out of the GDEs and mounted onto the rotating sample holder. The 2-D radiographs were recorded on an 11-megapixel camera with a projection angle step of 0.25° per radiograph. As the sample was rotated stepwise over the entire 180° range, 720 projections were taken with a 16-s exposure time for each projection. The accelerating voltage of the X-ray source was set to 40 kV. The radiographs had a resolution of 1 μm per Pixel. The image reconstruction and 3D rendering were conducted using the NRecon reconstruction software (Skyscan), which was part of the Micro-CT system.

2.2.3. Atomic force microscopy (AFM, conductive mode)

The AFM surface conductivity measurements were performed with a commercial AFM system (Multimode 8, Bruker). All images were taken with a combination of the so-called “PeakForce QNM”

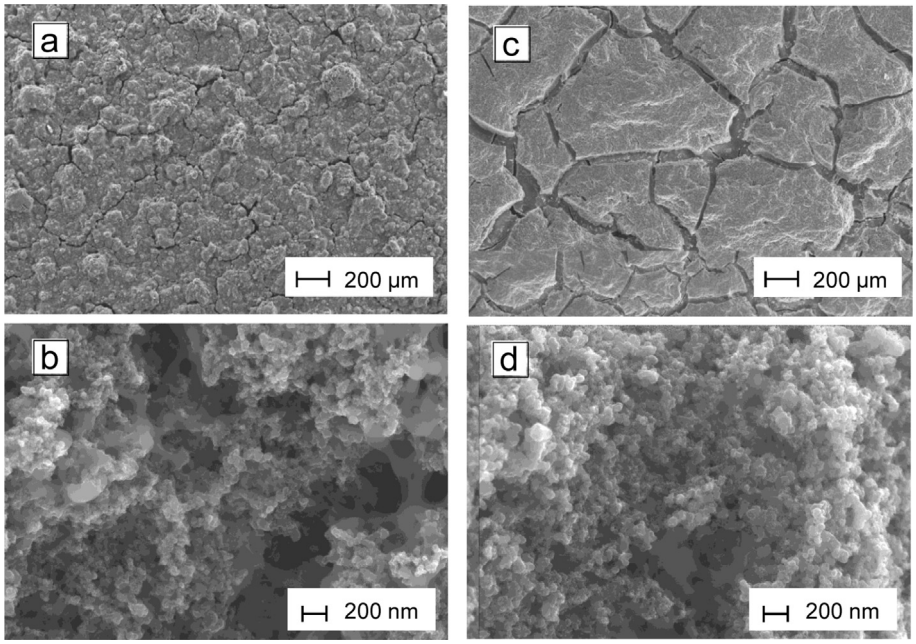

Fig. 1. SEM top view images of the sprayed and coated catalyst layers. Figures (a, b) present different magnifications 100× and 70,000× of the surface of sprayed catalyst layer. Figures (c, d) present different magnifications 100× and 70,000× of the surface of coated catalyst layer.

and "PeakForce TUNA" tapping modes of the AFM. The cantilever is oscillated below resonance frequency. This results in a continuous series of force–distance curves. The peak force is kept constant for direct force control and the surface conductivity is extracted and quantified from the force distant curve at each pixel within an image. A more detailed description of the AFM surface conductivity measurements can be found in Refs. [24,25].

2.3. Electrochemical characterization of GDEs in single cell tests

AB-PBI membranes (fumapem AM, Fuma-Tech) were doped with phosphoric acid by immersion in concentrated phosphoric acid (Carl Roth) at 120 °C for 6 h. During this process, the weight of the membrane increased by 300% (corresponding to a chemical formula AB-PBI·$6H_3PO_4$). The MEAs were prepared by placing the

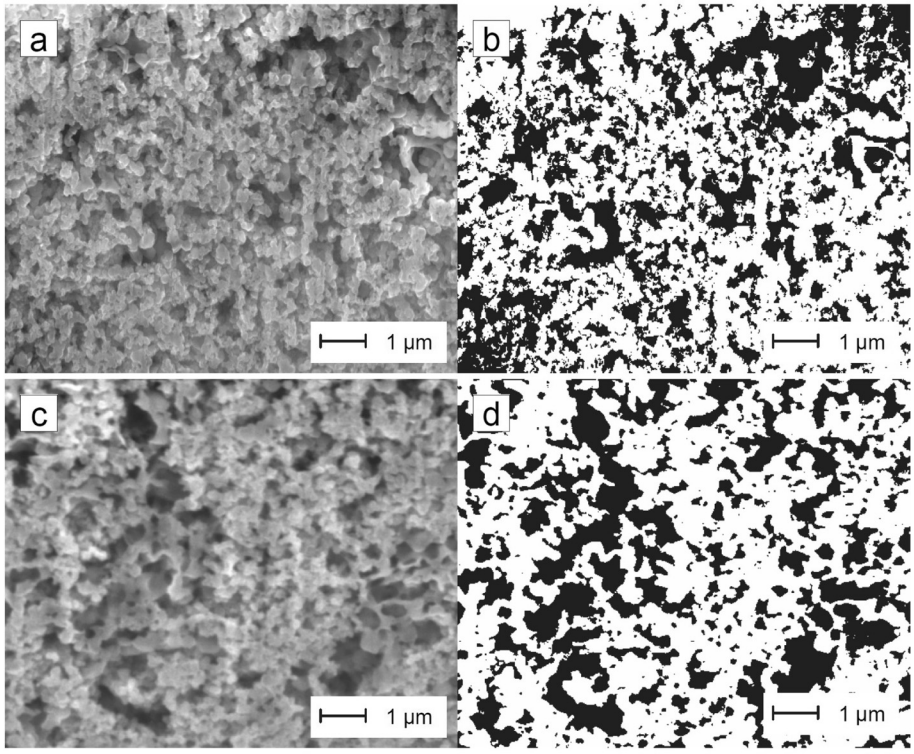

Fig. 2. SEM/FIB cross-sectional images and their threshold counterparts of the sprayed (a, b) and coated (c, d) catalyst layer at a magnification of 65,000×.

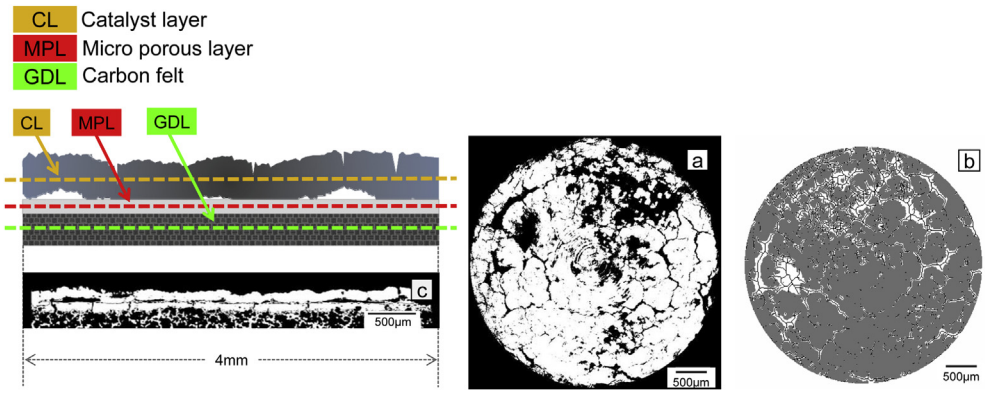

Fig. 3. X-ray microtomography images of the sprayed electrode. (a): In-plane cross-sectional image in the *XY*-plane of the Catalyst layer, (b) crack distribution in the catalyst layer, (c): Through-plane cross-sectional image in the *YZ*-plane.

GDEs in direct contact with the H_3PO_4-doped AB-PBI membranes in single cells without hot-pressing. Including gaskets (PTFE from Bohlender), sub-gaskets (PEEK from Victrex), metallic bipolar plates with single serpentine flow-fields (1 mm × 1 mm in dimension), and aluminum plates equipped with heating cartridges, the single cells with an active area of 4 cm^2 were assembled. The MEAs were compressed by 32% of the total thickness of individual components to keep a constant contact pressure. The cell performance was studied at 160 °C and ambient pressure using pure hydrogen and air as reactants. Stoichiometric mass flows of hydrogen ($\lambda = 1.4$) and air ($\lambda = 2$) were used for current densities equal to or greater than 200 mA cm^{-2}. Gas flows were fixed for lower current densities up to $j = 200$ mA cm^{-2}. Polarization curves were recorded by increasing the current density stepwise from zero (open circuit) up to 800 mA cm^{-2} or until the cell voltage dropped below 300 mV. Cell internal resistances were determined by measuring AC impedances at 1 kHz with an MR 2212W impedance meter (Schütz Meßtechnik).

3. Results and discussion

3.1. Macro-, microstructure and PTFE distribution of the electrodes

The combination of complementary methods SEM, Micro-CT, and AFM enables a comprehensive study of the macro- and microstructure as well as the PTFE distribution of the catalyst layer. SEM has a high resolution for investigating surfaces and cross-sections; however it requires the preparation of a dedicated cross-sectional sample. Micro-CT images the sample in a non-destructive fashion and therefore sample preparation artifacts can be avoided. With Micro-CT a macroscopic area of the sample can be investigated; whereas SEM studies are limited to small areas. The PTFE wires in the catalyst layer can be observed with SEM, though a quantitative distribution of PTFE particles requires AFM conductivity measurements.

SEM images of the sprayed and coated catalyst surfaces are shown in Fig. 1. On the micrometer scale (magnification of 100×), differences in the surface morphology are clearly visible. The sprayed electrode shows a rough surface (Fig. 1a) covered with islands up to 50 µm in diameter, and between these islands fine hairline cracks are present. The scenario appears different with the coated catalyst layer, which displays (Fig. 1c) a complete network of deep shrinkage cracks. The surface consists of many individual clots with sharp edges of 0.5–2 mm in diameter (Fig. 1c). On the nanometer scale (magnification of 70,000×), the two samples have similar surface morphology (Figs. 1b and d). The high-resolution images of both samples show agglomerates of individual PTFE particles and PTFE wires connected to Pt/C catalyst. Since it is not possible to evaluate the electrode structure solely based on surface images, we cut the catalyst layers with an FIB and created cross-sections as shown in Fig. 2. The sprayed (Fig. 2a) and coated (Fig. 2c) electrodes show comparable pore-sizes and pore-distribution within the catalyst layers. To calculate the pore volume, the brightness of each image was first adjusted to achieve the same brightness and then a threshold was applied as described in Ref. [26]. The sprayed electrode (Fig. 2b) has more small pores but

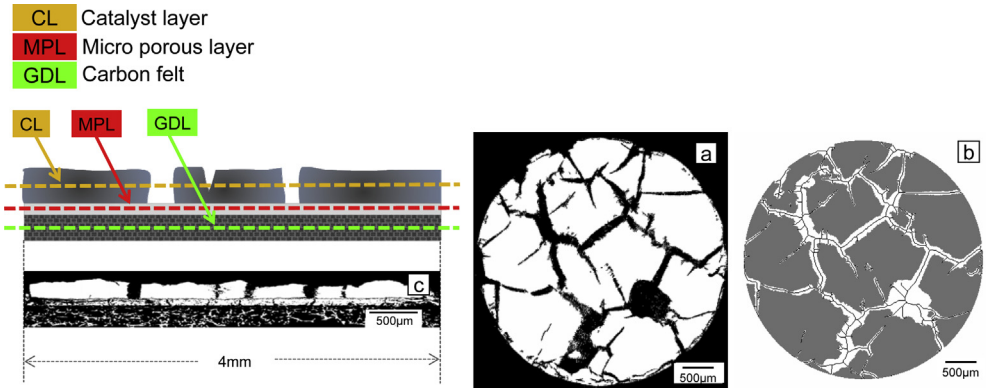

Fig. 4. X-ray microtomography images of the coated electrode. (a): In-plane cross-sectional image in the *XY*-plane of the catalyst layer, (b) crack distribution in the catalyst layer, (c): Through-plane cross-sectional image in the *YZ*-plane.

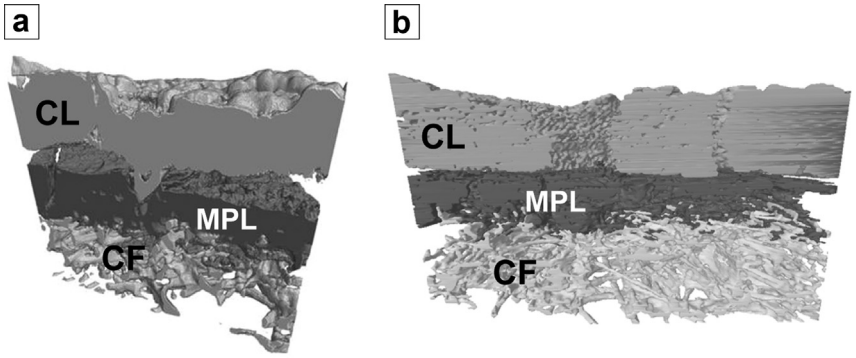

Fig. 5. 3D rendering of the X-ray microtomography data (a) sprayed electrode (b) coated electrode. CL, MPL, and CF stand for catalyst layer, microporous layer, and carbon felt, respectively.

fewer large pores compared with the coated electrode (Fig. 2d); however the volumes of pores are both about 40%.

Compared with the SEM/FIB method, the sample preparation for X-ray microtomography is much more straightforward, requiring only a section of the electrode be punched out from the GDE. The technique is capable to produce in-plane and through-plane images of the electrodes (Figs. 3 and 4) in a non-destructive fashion. The gray-scale tomograms display the variations in X-ray attenuation by different materials in the GDE, with brighter part of the tomogram indicating higher X-ray absorption. The attenuation coefficient of X-rays is proportional to the number of electrons in a material. Due to non-monochromatic radiation inside the μ-CT the exact attenuation coefficient is difficult to calculate. Exemplified for an X-ray energy of 40 keV (calculated with XOP), platinum has an attenuation coefficient of 247 cm^{-1}, much higher than that of carbon (0.05 cm^{-1}) and PTFE (0.08 cm^{-1}). Therefore, the catalyst layer is easily distinguishable from the microporous layer (MPL) and the carbon felt of the GDE because of the presence of platinum there. Although there is only a slight difference between the attenuation coefficients of carbon and PTFE, the individual layers of the carbon felt substrate and the MPL could also be differentiated from each other because of the finely distributed PTFE binder in the MPL. This allows for detailed analysis of the layer thicknesses and internal structures of the GDE from the X-ray microtomography images. Additionally, though-plane cross-sections are shown in Figs. 3c and 4c. Compared with the coated catalyst layer with its straight segments, the sprayed one appears much more heterogeneous, e.g. it contains voids and void clusters of different shapes and sizes (Fig. 3a and c) consistent with the SEM studies. The catalyst layer is partially delaminated from the MPL (Fig. 3c) due to the fact that the solvent of the suspension drops on the surface quickly evaporated after less than one minute for each layer.

The situation is different with the coating process, in which it takes more than 24 h before the catalyst layer is completely dried and the paste has enough time to settle. We therefore observe no voids between the catalyst layer and MPL for the coated GDE (Fig. 4c). However, because of the high liquid content of the catalyst ink when it is deposited via spraying, the catalyst penetrates into the MPL. According to the SEM studies, the coated catalyst layer shows a complete network of shrinkage cracks. The cracks go all the way though the catalyst layer. The clots are completely disconnected from each other as seen in Fig. 4c. The distance between these individual clots can be up to 50 μm.

The crack density is defined as the total length of cracks divided by the area as described in Ref. [23]. If the total sample area is considered, both electrodes can be investigated regarding the difference in crack length (Figs. 3b and 4b). The other dimension, i.e. the gap width of the cracks, can be evaluated, if the calculated area is the total area of cracks inside the sample area. For the coated electrode the crack density is 3.0 mm^{-1} and the gap width is 14.0 mm^{-1}. The sprayed electrode shows values of 6.3 mm^{-1} and 30.7 mm^{-1}. For the sprayed electrode, both densities are almost doubled in comparison to the coated electrode. For both electrodes, one representative layer was evaluated, as the cracks are homogenous over the electrode thickness. As the gray value threshold is user defined, there is a given uncertainness. The difference of adjusting the lower limit for threshold by optimizing the electrode and also the non-material, i.e. the cracks, gives a total error of one

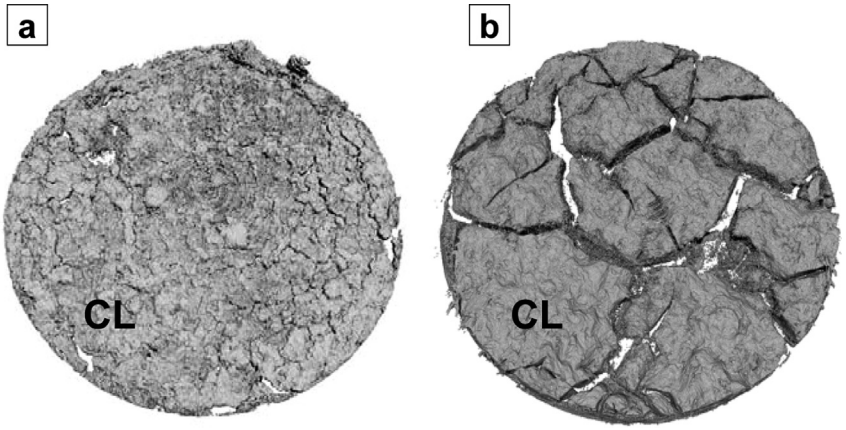

Fig. 6. 3D rendering of the X-ray microtomography data for the electrode surfaces (a) sprayed electrode (b) coated electrode. CL stands for catalyst layer.

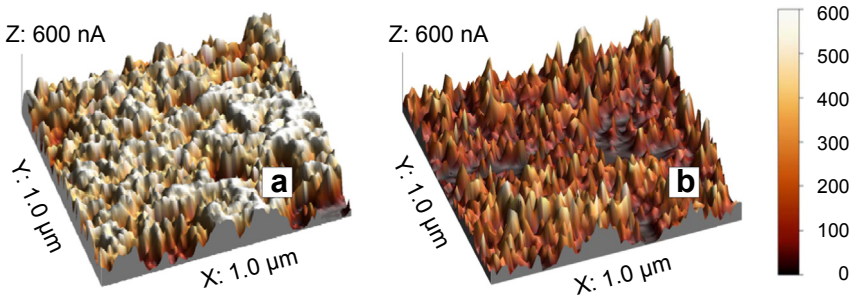

Fig. 7. Locally resolved current maps of (a) sprayed and (b) coated GDEs measured with the conductive AFM. The scan area is 1 µm × 1 µm.

pixel. That means when choosing the upper and lower limit for binarisation creates an error of ±0.5 µm for the sprayed electrode and an uncertainness of ±1 µm per pixel for the coated electrode.

From the through-plane cross-sections in Figs. 3c and 4c the actual thicknesses of the individual layers in the GDE could be determined. Neglecting the cracks in the MPL filled with catalyst ink, the measured catalyst layer thicknesses are 142 ± 15 µm and 168 ± 20 µm for the sprayed and coated electrodes, respectively. Since we used the same commercial GDL for both samples, we obtained comparable thickness values for the MPL (110 ± 11 µm) and the carbon felt (264 ± 19 µm).

A 3D rendered image of the sprayed GDE (Fig. 5a) shows that the catalyst ink penetrates the MPL and fills up an exemplary large crack of MPL. A similar effect was observed for material of the MPL inside the GDL from Pfrang et al. [27]. Again, voids between the catalyst layer and the MPL are present with the sprayed GDE. In comparison, the clots of the coated catalyst layer completely laminate the MPL surface (Fig. 5b). For better visual impressions of the sprayed and coated electrodes, we also generated top-view 3D images of the catalyst layer surfaces (Figs. 6a and b).

Locally resolved current distributions of the sprayed (Fig. 7a) and coated (Fig. 7b) electrode surfaces were obtained with the conductive AFM. We selected an images size of 1 µm × 1 µm. Bright regions with high surface current represent catalyst (Pt/C) rich areas. Since PTFE agglomerates and gas pores have lower conductivities than platinum and graphite, regions with a high PTFE content or many gas pores appear darker. Because of their distinctive spherical shape, the PTFE particles usually appear as dark round spots with a size of approximately 100 nm in the image (Fig. 7a). The average surface conductivity of the sprayed electrode is larger than the coated electrode. A possible explanation is the PTFE distribution within the catalyst layer, which is sensitive to the electrode preparation process. During spraying, the catalyst ink, a homogeneous mixture of PTFE and Pt/C, dries layer by layer on the GDL and leads to a uniform PTFE distribution. In contrast, the coating process takes 24 h for the paste to dry, during which the lighter PTFE particles (2.08 g cm^{-3} compared to a mean density >2.3 cm^3 for Pt/C; particles very rich in Pt might approach the 21.45 g cm^{-3} of Pt) are likely to migrate to the top region of the catalyst layer and form a nonconductive "skin" on the electrode surface. The effect could be seen more quantitatively in the histogram of the surface current distribution presented in Fig. 8. Note the high-resistance region (the first current bin with AFM current <25 nA) amounts to ~25% of the total surface area of the coated electrode. With the sprayed electrode, on the other hand, the percentage of the insulating area is only 3% and the current distribution is skewed towards high current.

3.2. Influence of the morphology of the electrodes on the fuel cell performance

The sprayed and coated electrodes were incorporated into MEAs and were evaluated in single cell tests. After a break-in period of around 120 h, the two MEAs demonstrated similar cell performance (Fig. 9). The MEA with the sprayed electrode delivered a peak power density of 230 mW cm^{-2}, and the MEA with the coated electrodes 220 mW cm^{-2}. At a current density of 200 mA cm^{-2}, the cell voltages were 588 mV and 580 mV for the sprayed and coated MEAs, respectively. The polarization curves are comparable to those reported by Wannek et al. [4,28] with MEAs fabricated and operated in

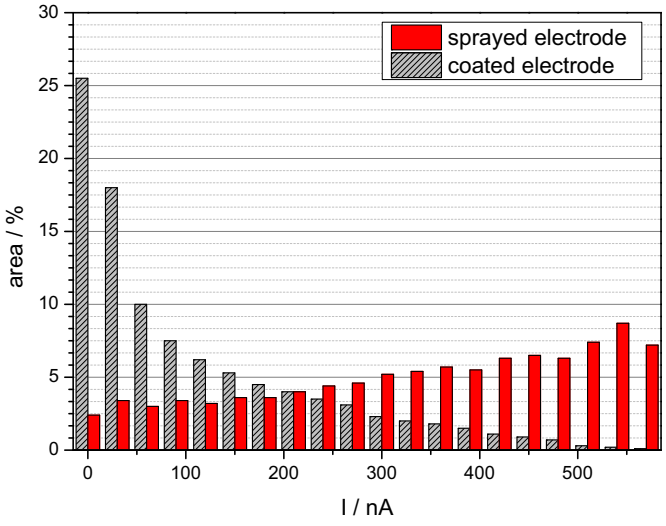

Fig. 8. Histograms of the locally resolved current measured on the sprayed (full bars) and coated (hatched bars) electrodes (using input data from Fig. 7).

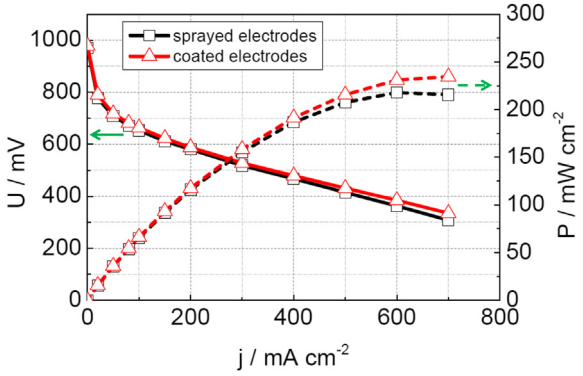

Fig. 9. Fuel cell performance of ABPBI-based MEAs with sprayed and coated electrodes after 120 h break-in procedure, operated at 160 °C, ambient pressure and λ = 1.4/2.

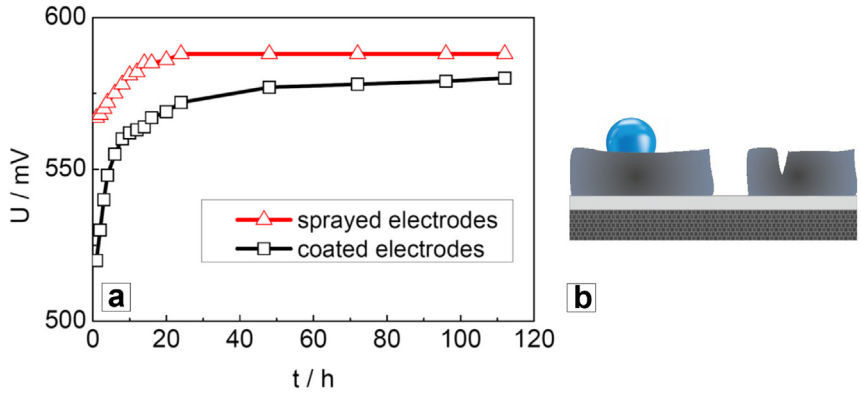

Fig. 10. Start-up behavior of MEAs with sprayed and coated electrodes: (a) Cell voltage of the first 120 h of operation with a fixed current density $j = 200$ mA cm^{-2}; (b) schema to illustrate the poor wettability between phosphoric acid and the coated GDE.

similar manners (coated electrodes in those studies). Furthermore, an internal cell resistance of 60 mΩ cm^2 was measured for both MEAs.

However, we did observe a strong effect of the PTFE distribution in the electrodes on the start-up behavior of the MEA, as shown in Fig. 10a. After 1 h of operation, the fuel cell with the sprayed MEA reached a cell voltage of 570 mV at the current density of 200 mA cm^{-2}, which is already close to the steady-state cell voltage. The MEA with the coated electrode started up much slower and took more than 20 h to reach 570 mV. This behavior is consistent with the AFM surface conductivity measurements (Fig. 7). As previously discussed, the coating process tends to form a PTFE "skin" at the surface of the catalyst layer. This PTFE-rich layer affects not only the surface conductivity but also the wettability of the catalyst layer (Fig. 10b). The high PTFE content creates a hydrophobic electrode surface, which slows down the phosphoric acid uptake during the start-up period of the MEA.

Despite the strong influence of electrode macrostructure and the surface conductivity on the start-up behavior, the steady-state fuel cell performance is hardly affected at all. The microstructure (pore volume) of the electrode appears to dominate the steady-state performance. The slow start-up behavior observed with the coated electrode only represents the initial stage for the phosphoric acid to overcome the hydrophobic PTFE barrier. Once the phosphoric acid has migrated into the GDEs, the MEAs with sprayed and coated electrodes have similar microscopic acid distributions. In HT-PEMFCs, the phosphoric acid distribution inside the MEA determines the triple phase boundary between catalyst, electrolyte, and reactant gases, which is the dominating factor for the cell performance [29].

The absence of liquid water in the system is one of the most important differences compared with low-temperature PEMFCs. Water management is crucial for low-temperature PEMFCs, and consequently the macrostructure [11], the distribution of the polymer binder [30] in the electrodes, and the structure of the microporous layer [13] all have strong effects on the cell performance. In contrast, for HT-PEMFC, the GDL and MPL in the MEA play only a minor role for the cell performance [31]. The fact that the MEA performance of these sprayed and coated electrodes is more reproducible than typical handmade low-temperature PEMFC electrodes [11] indicates the robustness of the HT-PEMFC performance against structural variations due to electrode preparation.

4. Conclusions

The combination of the complementary methods SEM, Micro-CT, and AFM enables comprehensive studies of the micro- and macrostructure of the HT-PEMFC electrodes. This leads to a deeper understanding of the influence of the morphology and the PTFE distribution of the catalyst layer on the start-up behavior and steady-state performance of HT-PEMFCs.

Unlike low-temperature PEMFCs, the electrode macrostructure of HT-PEMFCs has no significant impact on the steady-state performance of the fuel cell due to the absence of liquid water in the system. Water is not required for the ionic conductivity and flooding of the catalyst layer's pores with water does not occur.

However, the distribution of phosphoric acid as the liquid electrolyte in the MEA is crucial for the performance of HT-PEMFCs. Therefore, a PTFE-rich surface of the catalyst layer formed by a slow drying process delays the phosphoric acid ingress in the electrodes and hinders the start-up performance. The microstructure plays the most important role for the formation of the triple phase boundary in HT-PEMFCs between catalyst, phosphoric acid, and reactant gases; consequently it determines the activity of the electrodes and the cell performance. These results demonstrate the robustness of HT-PEMFCs against electrode macrostructure variations due to subtle differences in MEA preparation.

Acknowledgments

This work was supported by the Impuls- und Vernetzungsfonds der Helmholtz Gesellschaft (Young Investigator Group project VH-NG-616).

References

[1] J.S. Wainright, J.-T. Wang, D. Weng, R.F. Savinell, M. Litt, J. Electrochem. Soc. 142 (1995) L121.
[2] W. Lehnert, C. Wannek, R. Zeis, Innov. Fuel Cell. Technol. (2010).
[3] Y.-H. Cho, S.-K. Kim, T.-H. Kim, Y.-H. Cho, J.W. Lim, N. Jung, W.-S. Yoon, J.-C. Lee, Y.-E. Sung, Electrochem. Solid State Lett. 14 (2011) B38.
[4] C. Wannek, W. Lehnert, J. Mergel, J. Power Sources 192 (2009) 258.
[5] J.O. Park, K. Kwon, M.D. Cho, S.-G. Hong, T.Y. Kim, D.Y. Yoo, J. Electrochem. Soc. 158 (2011) B675.
[6] J. Lobato, P. Cañizares, M.A. Rodrigo, J.J. Linares, F.J. Pinar, Int. J. Hydrogen Energy 35 (2010) 1347.
[7] M. Mamlouk, K. Scott, Int. J. Hydrogen Energy 35 (2010) 784.
[8] P. Mazur, J. Malis, M. Paidar, J. Schauer, K. Bouzek, Desalin. Water Treat. 14 (2010) 101.
[9] J.-H. Kim, H.-J. Kim, T.-H. Lim, H.-I. Lee, J. Power Sources 170 (2007) 275.
[10] P. Mazúr, J. Soukup, M. Paidar, K. Bouzek, J. Appl. Electrochem. 41 (2011) 1013.
[11] H.-R. Jhong, F.R. Brushett, P.J.A. Kenis, Adv. Energy Mater. 3 (2013) 589.
[12] H.-R. Jhong, F.R. Brushett, L. Yin, D.M. Stevenson, P.J.A. Kenis, J. Electrochem. Soc. 159 (2012) B292.
[13] W.-M. Yan, D.-K. Wu, X.-D. Wang, A.-L. Ong, D.-J. Lee, A. Su, J. Power Sources 195 (2010) 5731.
[14] D.S. Hwang, C.H. Park, S.C. Yi, Y.M. Lee, Int. J. Hydrogen Energy 36 (2011) 9876.
[15] N. Rajalakshmi, K.S. Dhathathreyan, Chem. Eng. J. 129 (2007) 31.
[16] S. Litster, G. McLean, J. Power Sources 130 (2004) 61.

[17] K. Seidenberger, M. Klages, F. Wilhelm, J. Scholta, ECS Trans. 42 (2012) 179.
[18] R. Zeis, A. Mathur, G. Fritz, J. Lee, J. Erlebacher, J. Power Sources 165 (2007) 65.
[19] A. Kamat, A. Huth, O. Klein, S. Scholl, Fuel Cells 10 (2010) 983.
[20] E. Gülzow, M. Schulze, N. Wagner, T. Kaz, R. Reissner, G. Steinhilber, A. Schneider, J. Power Sources 86 (2000) 352.
[21] M.D. Gasda, R. Teki, T.-M. Lu, N. Koratkar, G.A. Eisman, D. Gall, J. Electrochem. Soc. 156 (2009) B614.
[22] P.K. Sinha, P. Halleck, C.-Y. Wang, Electrochem. Solid State Lett. 9 (2006) A344.
[23] A. Pfrang, D. Veyret, G.J.M. Janssen, G. Tsotridis, J. Power Sources 196 (2011) 5272.
[24] E. Aleksandrova, R. Hiesgen, K. Andreas Friedrich, E. Roduner, Phys. Chem. Chem. Phys. 9 (2007) 2735.
[25] R. Hiesgen, I. Wehl, E. Aleksandrova, E. Roduner, A. Bauder, K.A. Friedrich, Int. J. Energy Res. 34 (2010) 1223.
[26] K.J. Lange, H. Carlsson, I. Stewart, P.-C. Sui, R. Herring, N. Djilali, Electrochim. Acta 85 (2012) 322.
[27] A. Pfrang, S. Didas, G. Tsotridis, J. Power Sources 235 (2013) 81.
[28] C. Wannek, I. Konradi, J. Mergel, W. Lehnert, Int. J. Hydrogen Energy 34 (2009) 9479.
[29] F. Mack, T. Morawietz, R. Hiesgen, D. Kramer, R. Zeis, ECS Trans. 58 (2013) 881.
[30] Z. Xie, T. Navessin, K. Shi, R. Chow, Q. Wang, D. Song, B. Andreaus, M. Eikerling, Z. Liu, S. Holdcroft, J. Electrochem. Soc. 152 (2005) A1171.
[31] S. Galbiati, Experimental Study of Polybenzimidazole Based High Temperature Polymer Electrolyte Fuel Cells, 2012 (PhD thesis).